# Low-temperature grown vertically aligned carbon nanotube array for an optimal infrared bolometer

**Qi Wang**[1]**, Yu Zheng**[2]**, Changjian Zhou**[1,3] ⓘ**, Mansun Chan**[4] **and Cary Y Yang**[2]

[1] School of Microelectronics, South China University of Technology, Guangzhou 510640, People's Republic of China
[2] Center for Nanostructures, Santa Clara University, Santa Clara, CA, United States of America
[3] Pazhou Lab, No. 70 Yuean Road, Haizhu District, Guangzhou, 510330, People's Republic of China
[4] Department of Electronic and Computer Engineering, Hong Kong University of Science and Technology, Kowloon, Hong Kong

E-mail: zhoucj@scut.edu.cn

## Abstract

Vertically aligned carbon nanotube (VACNT) arrays have been explored as an absorber of thermal-type photodetectors. A long and dense VACNT array absorbs a wide spectral range of incident light with high absorption rate, but has a high thermal mass that results in a low response speed. To achieve a small thermal mass, a shorter and less dense VACNT array is needed. In addition, the high temperature needed to grow the VACNTs is detrimental to the functional sensing materials of the photodetector. The height, density, and growth temperature of VACNTs need to be optimized to achieve a working absorber that has high absorption rate and a high response speed. In this work, a low-temperature plasma enhanced chemical vapor deposition process is used to prepare various VACNT arrays with different heights and densities by controlling the CNT growth parameters. The absorption coefficients of the resulting samples are measured with Fourier transform infrared spectroscopy. An effective medium theory (EMT) is adopted to establish a working model of the VACNTs. Using experimentally extracted CNT density and height as fitting parameters, the EMT model is fitted to obtain theoretical absorption coefficients, which are found to be comparable to the experimentally measured absorption coefficients. Our experimental and theoretical investigations pave the way for future studies to integrate CNTs with infrared photodetectors.

Supplementary material for this article is available online

Keywords: low-temperature grown, CNT, infrared absorption

(Some figures may appear in colour only in the online journal)

## 1. Introduction

Room-temperature infrared photodetectors based on the photothermal effect have received much attention due to their low cost, small size, and improved detectivity in recent years [1]. However, the core detection materials used for photo-thermal infrared detectors, such as vanadium oxide, amorphous silicon, and pyroelectric materials, have relatively low infrared absorption coefficients [2, 3]. Therefore, it is necessary to prepare an additional infrared absorption layer or infrared absorption structure to achieve enhanced infrared absorption and light-to-heat conversion. At present, there are two main approaches: one is to form an optical cavity under the detector [4]. Typical examples include bolometers based on vanadium oxide and amorphous silicon. This structure requires the formation of a cavity with a height 1/4 of wavelength below the detection film [4]. Raytheon's vanadium oxide-based bolometer uses this structure and obtains an

average absorption rate of ∼80% in the long-wavelength infrared band [5]. However, the high absorption rate of the optical resonant cavity is only obtained in the narrow band near the resonance peak [6]. Another common approach is to prepare black absorbing materials such as black gold, black platinum, black silicon, or carbon black coatings on the upper surface of the detector [4, 7–9]. The National Institute of Standards and Technology used a thermal evaporation process to prepare a porous black gold thin film on a 60 $\mu$m single-crystal LiTaO$_3$ substrate [8]. Lang *et al* prepared a 1 $\mu$m porous black platinum film with the electrochemical method, and obtained ∼90% absorption rate at a wavelength of 10 $\mu$m [4]. The black coating can provide a high absorption rate in a wide spectral range, but its fragile structure and rough surface make it difficult to be adopted in two-dimensional array structures that require subsequent processes such as patterning and selective etching. In addition, to obtain a sufficiently high absorption rate, the thickness of the black coating layer is 1–3 $\mu$m, which leads to a large thermal capacity and adversely affects the response speed of the infrared detector [10].

In recent years, researchers have begun to explore new types of infrared absorption structures and materials, such as plasma surface resonance structures [11], nanoparticles [12] and carbon nanotube arrays [13–20]. Suen *et al* prepared electrode resonance structures on LiNbO$_3$ substrates, similar to optical resonators [11]. Through the design of the surface electrode pattern, a narrow-band high-absorption characteristic centered on a specific detection wavelength can be obtained. Wang *et al* demonstrated the possibility of using Ti$_2$O$_3$ nanoparticles as an efficient photothermal material by taking advantage of both its narrow bandgap and nanoscale features [12]. The narrow-bandgap enables Ti$_2$O$_3$ nanoparticles to absorb the full solar spectrum, while the nanoscale features further enhance the absorption efficiency. Tomlin *et al* described a microfabricated bolometer with vertically aligned carbon nanotube (VACNT) absorbers [13]. Lehman *et al* reported carbon nanotube-based black coatings [14]. Nandi *et al* developed a novel spray coating and transfer method for fabricating a suspended bolometer of vanadium oxide-coated multi-walled carbon nanotubes [15]. Jönsson *et al* used *in situ* laser reflectivity measurements to monitor the growth of MWCNT films during plasma enhanced chemical vapor deposition (PECVD) [16]. Theocharous fabricated a 150 $\mu$m thick CNT array on a 60 $\mu$m thick pyroelectric single-crystal LiTaO$_3$ [17]. The resulting pyroelectric infrared detector achieved a uniform responsivity in the spectral range of 0.8–24 $\mu$m. Mizuno reported results on a vertical single-walled CNTs array 460 $\mu$m tall on a silicon wafer, which showed an absorption rate greater than 98% in a wide spectral range of 5–12 $\mu$m [18]. It has been found that VACNT arrays can absorb incident light almost perfectly in a wide spectral range from UV (200 nm) to far infrared (200 $\mu$m) [18]. More importantly, compared with the traditional black materials, the absorption rate of a VACNT array is almost independent of wavelength in the entire measurement spectrum range. These characteristics are ideal for absorbing radiation, such that VACNTs can effectively convert light into heat, which is of great significance for solar collectors and infrared heat detectors. Ideally, the VACNT arrays absorb the IR light and induce a temperature increase of the sensing element, which could be a thermopile, thermistor, or pyroelectric photodetector. Further, the excellent thermal conductivity of the CNT absorber can accelerate the heat conduction from the CNT to the sensing element, which helps to increase the response speed of the photodetector.

Although high absorption rate can be obtained with VACNT arrays, lengths exceeding 100 $\mu$m in certain cases exhibit a relatively large heat capacity, resulting in low response speed and a small responsivity. Moreover, the high growth temperature is detrimental to the functional sensing materials as it causes depolarization of the pyroelectric material and/or recrystallization of the amorphous thermo-resistive materials. Therefore, balancing the thermal mass requirement, absorptivity and process thermal budget when integrating CNTs and infrared photodetectors requires further investigation. And producing an efficient infrared absorption layer with a small heat capacity that can be integrated into a two-dimensional array structure, while achieving a high absorption rate in a wide spectral range, is yet to be realized. In this study, we grow CNT samples at low temperature using a PECVD reactor and perform quantitative analysis to better understand the infrared absorption behavior of VACNT arrays. We prepare the VACNT arrays with low thermal mass and carry out experiments to verify our models for the absorption coefficients of the grown VACNT arrays.

This paper presents a new perspective for IR sensor application of CNT arrays by focusing on the absorption phenomena. In previous studies on this subject [18, 21, 22], analysis of the dependence of the absorption coefficient on the array fill factor was lacking. For example, Ye *et al* [21] presented the absorption coefficients of three VACNT films, with the experimental data and fitted results from effective medium theory (EMT) without considering the fill factor. Further, previous studies mainly focused on how to achieve high absorption by using tall CNT arrays, while the process requirements such as low temperature and sensor performance such as low thermal mass were often overlooked [18, 21, 22]. The present study takes into account growth temperature, thermal mass, as well as both the fill factor and the alignment factor of the CNT array, and can serve as the basis for future integration of CNTs into photothermal infrared detectors.

## 2. Experimental and calculation methods

### 2.1. Experiment method

Chemical vapor deposition is the most commonly used method for preparing CNTs, and the introduction of plasma could reduce the growth temperature, and achieve VACNTs. Therefore, in this study, PECVD with a Seki AX5200M reactor is employed to grow the VACNT arrays on a double-polished 100 mm silicon wafer. To prevent silicide formation during the growth stage, a 10 nm thick ZrO$_2$ dielectric layer is deposited on the growth side of the silicon wafer using atomic
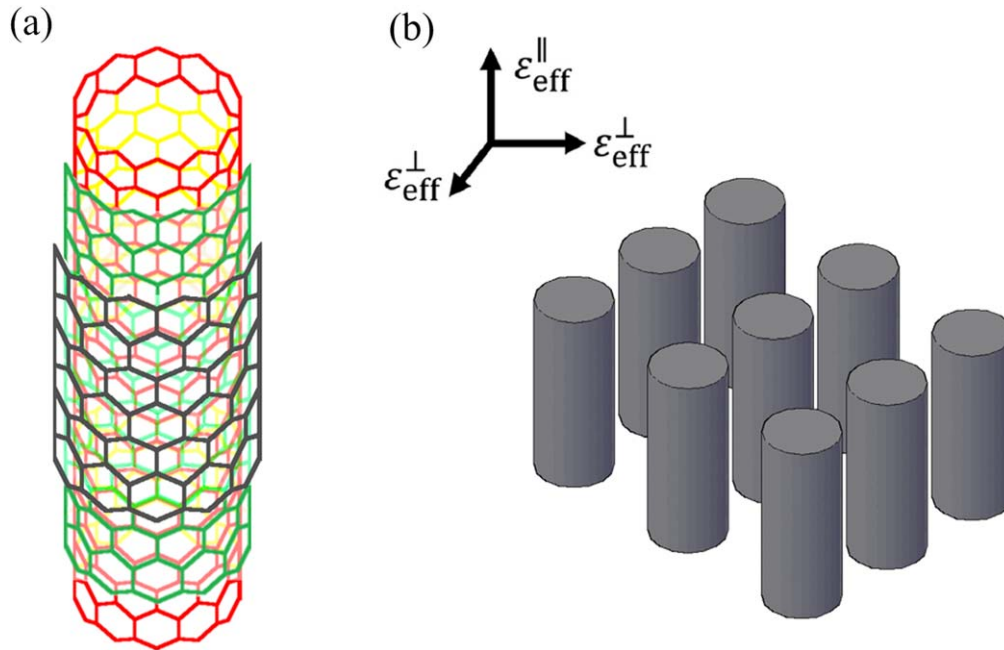
**Figure 1.** (a) Schematic diagram of an individual multi-walled CNT. (b) Solid cylindrical graphite rod model of a VACNT array, where the perpendicular out-of-plane and in-plane components of the anisotropic dielectric function are indicated by referring to the rod axis.

layer deposition under 200 °C. Then a 2 nm thick Ni catalyst is prepared on top of the $ZrO_2$ layer using electron-beam evaporation under a high vacuum of $1 \times 10^{-7}$ Torr. The Ni deposition rate is controlled to be $0.2$ Å s$^{-1}$ and the thickness is monitored with a crystal quartz microbalance *in situ*. The sample is loaded onto an alumina stage located in the center of the growth chamber. The stage temperature is first ramped up to the growth temperature and annealed for 10 min in $H_2:N_2 = 30$ sccm:10 sccm ambient. During the growth, the stage temperature is monitored using a dual-wavelength infrared temperature measuring system. It is noted that Maschmann *et al* used a pyrometer to measure the catalytic substrate surface temperature to study the heating effect of the plasma power [23]. In this study, the heating power is dynamically controlled to maintain a constant stage temperature. The growth is then initiated by introducing $CH_4$ at 35 sccm as the carbon source and igniting the 200 W plasma power. When the growth time is reached, both the plasma power and the $CH_4$ gas flow are shut down to prevent any unnecessary amorphous carbon formation on top of the CNT array. The sample is then cooled down to room temperature in $H_2$ at 50 sccm. By varying CNT growth temperature and time, we prepare VACNT array samples with different heights and densities.

We first measure the CNT's transmittance $T$, and then calculate its absorbance using $A = 1 - T$, assuming the reflectance of the sample is negligible which is reasonable for dark materials. We then use Fourier transform infrared (FTIR) spectroscopy (Bio Rad FTS 6000) to measure the transmittance of the sample. The instrument is a high-performance research-grade multi-range FTIR spectrometer capable of both rapid scan and step scan operation and covers the spectral range of 50 000–10 cm$^{-1}$. For dark materials, it is crucial to minimize or correct the typical sources of uncertainty, so a reference calibration is performed with a double-sided polished

Si substrate. We measure the transmittance of the bare silicon wafer $T_{sub}$ polished on both sides using FTIR and the transmittance of the sample $T_{sample}$ (CNT-substrate composite, figure S1), which is the product of the transmittances of the CNT film and the substrate, $T_{sample} = T_{CNT} \times T_{sub}$. Thus, the CNT transmittance $T_{CNT}$ can be obtained. Because the silicon wafers are measured under the same conditions, the errors caused by the instrument and the environment are eliminated.

We use the liquid-induced compaction (LIC) method to evaluate the density of the CNT samples, and then determine the fill factor $f$ [24]. The LIC method involves soaking the CNT samples thoroughly in ethanol and letting them dry in air so that the CNTs are aggregated. Different heights of CNTs correlates with different densities, which form different microstructures with LIC treatment. For low-density samples, a cellular structure is usually formed. For high-density CNTs, CNT islands are formed after densification.The LIC-processed CNT network is then used to estimate the density of CNT arrays. The fill factor will be used as an important parameter in the following analysis.

### 2.2. Method for calculating VACNT array absorption coefficient

The VACNT array film is an inhomogeneous medium because it consists of individual CNTs and voids [22]. To quantitatively analyze its absorption coefficients, we use the EMT [25, 26] to establish an approximate model of VACNTs. As shown in figure 1(a), each CNT in the array is modeled by a graphitic layer formed parallel to the growth direction. Essentially, the VACNT arrays can be regarded as a uniaxial medium with the optical axis parallel to the CNT axis. Thus, the Maxwell-Garnett approximation (MGA) [27] can be used. Garcia-Vidal proposed an EMT based on MGA to model a VACNT array [25]. A schematic of the model is shown in
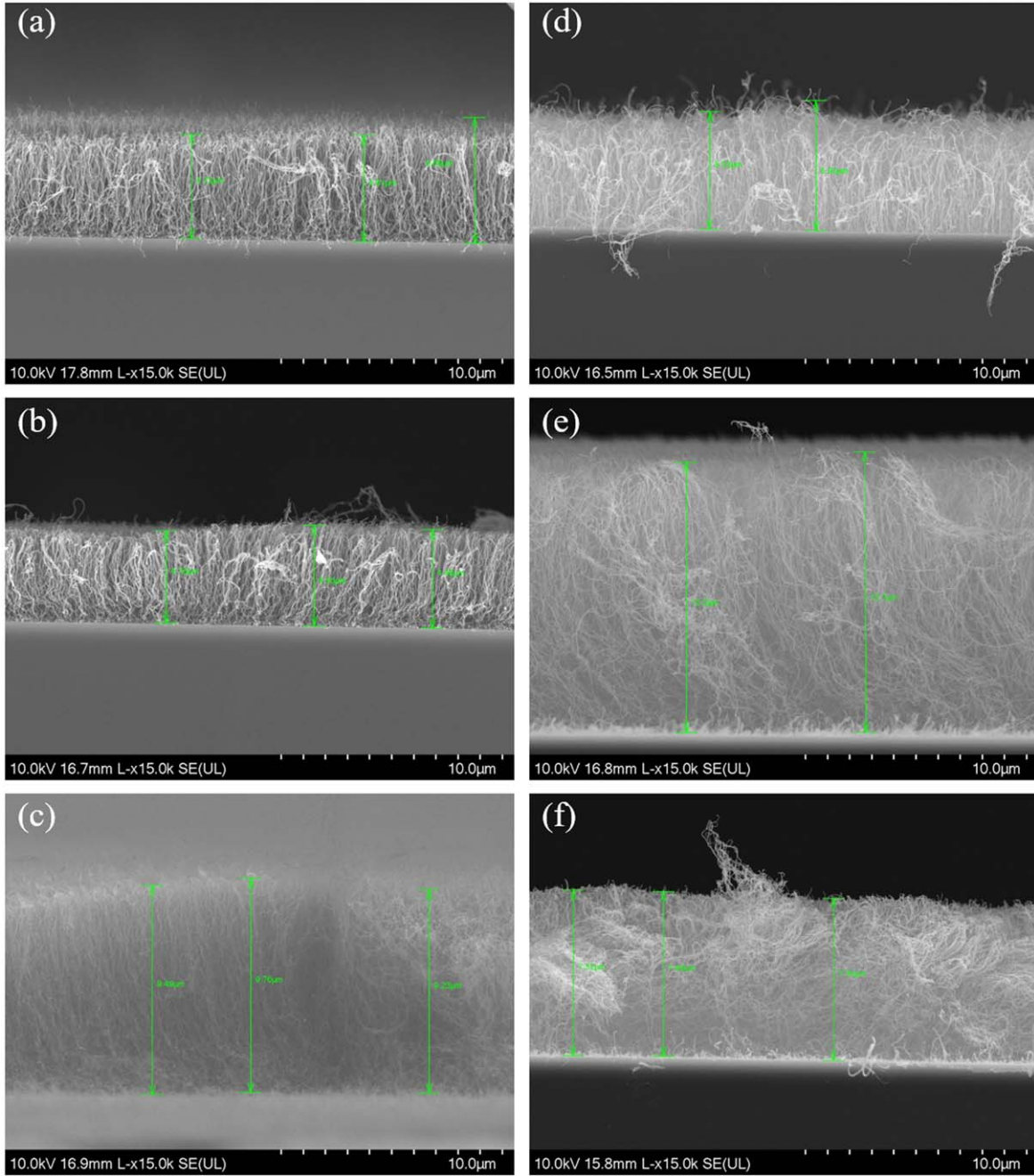
**Figure 2.** SEM images of carbon nanotubes under different growth conditions, with the heights marked in green. (a) 480 °C for 3 min, 4.81 $\mu$m. (b) 480 °C for 5 min, 4.46 $\mu$m. (c) 580 °C for 5 min, 9.47 $\mu$m. (d) 530 °C for 5 min, 5.33 $\mu$m. (e) 530 °C for 15 min, 12.2 $\mu$m. (f) 530 °C for 20 min, 7.45 $\mu$m.

figure 1(b), where each CNT is modeled as a solid graphite rod.

Based on this model of VACNT array, the optical constants of graphite are utilized to simulate the properties of CNTs [28]. The in-plane components of the dielectric function, $\varepsilon_{xx}$ and $\varepsilon_{yy}$, are for ordinary waves, in which the electric field is perpendicular to the optical axis, and are denoted by $\varepsilon_o$ or $\varepsilon_\perp$. The out-of-plane component ($\varepsilon_{zz}$) is for extraordinary waves, in which the electric field is parallel to the optical axis, and is denoted by $\varepsilon_e$ or $\varepsilon_\parallel$. Based on MGA and coordinate transformation, the effective dielectric functions of perfectly aligned CNT arrays can be expressed as [25, 29, 30]

$$\varepsilon_{\text{eff}}^\perp = \frac{\sqrt{\varepsilon_e \varepsilon_o}(1+f) + \varepsilon_{\text{vac}}(1-f)}{\sqrt{\varepsilon_e \varepsilon_o}(1-f) + \varepsilon_{\text{vac}}(1+f)}, \tag{1}$$

$$\varepsilon_{\text{eff}}^\parallel = f\varepsilon_o + (1-f)\varepsilon_{\text{vac}}, \tag{2}$$

where $\varepsilon_{\text{vac}} = 1$ is the vacuum dielectric function, and $\varepsilon_o = \varepsilon_\perp$ ($\varepsilon_e = \varepsilon_\parallel$) is the ordinary (extraordinary) dielectric function of graphite, $\varepsilon_{\text{eff}}^\perp$ ($\varepsilon_{\text{eff}}^\parallel$) the component perpendicular (parallel) to the CNT axis, and the fill factor $f$ ranges from 0 to 1, defined
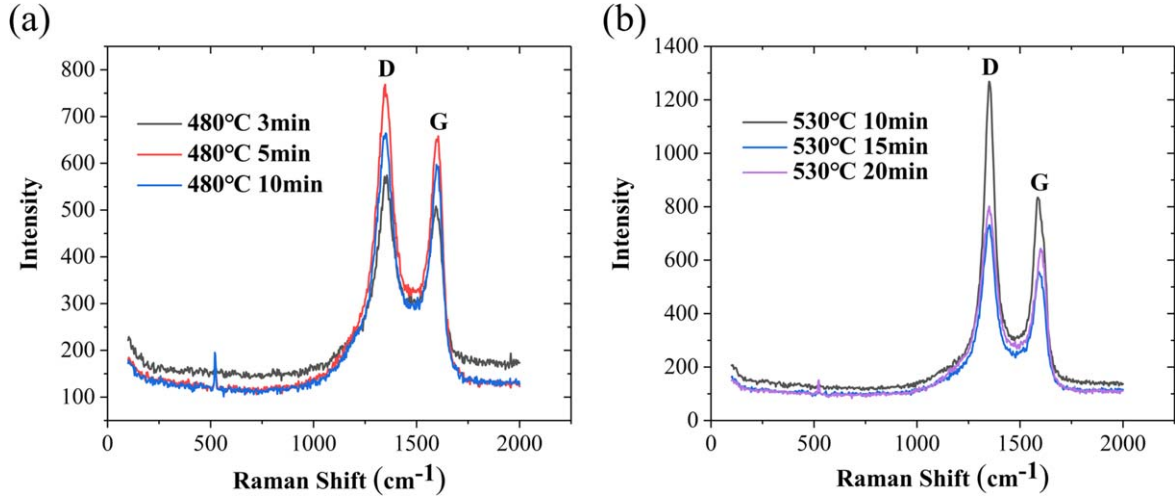
**Figure 3.** Raman spectra of (a) CNT samples grown at 480 °C and (b) CNT samples grown at 530 °C.

**Table 1.** Spectral data by Raman measurements for CNT arrays prepared under different conditions.

| Growth temperature (°C) | Growth time (min) | D center position (cm$^{-1}$) | G center position (cm$^{-1}$) | D peak intensity $I_D$ (a.u.) | G peak intensity $I_G$ (a.u.) | $I_D/I_G$ |
|---|---|---|---|---|---|---|
| 480 | 3 | 1356.17 | 1593.67 | 574.407 | 508.198 | 1.130 |
| 480 | 5 | 1347.59 | 1605.12 | 768.499 | 658.006 | 1.168 |
| 480 | 10 | 1350.45 | 1596.54 | 664.478 | 597.157 | 1.113 |
| 530 | 10 | 1350.45 | 1585.09 | 1268.41 | 834.741 | 1.520 |
| 530 | 15 | 1350.45 | 1590.81 | 731.471 | 556.501 | 1.314 |
| 530 | 20 | 1350.45 | 1599.4 | 801.874 | 643.392 | 1.246 |

within this model as the fraction of volume occupied by the graphite rods.

Considering the defects in sample preparation, such as random tilt and entanglement, the effect of the imperfect alignment of nanotubes on the dielectric function can be addressed by adding a weighting factor $x$ designated as alignment factor. The alignment factor of a perfectly vertically aligned CNT array is 1, and imperfect alignment corresponds to $x < 1$ [22]. The dielectric functions of fabricated VACNT arrays with different alignment factors are calculated from the following expressions [21, 29]

$$\varepsilon^{\perp}_{\text{VACNT}} = x\varepsilon^{\perp}_{\text{eff}} + (1 - x)\varepsilon^{\parallel}_{\text{eff}}, \tag{3}$$

$$\varepsilon^{\parallel}_{\text{VACNT}} = x\varepsilon^{\parallel}_{\text{eff}} + (1 - x)\varepsilon^{\perp}_{\text{eff}}. \tag{4}$$

The absorption coefficient ($\alpha_\lambda$) in the VACNT films at normal incidence can then be obtained [31]

$$\alpha_\lambda = 4\pi k/\lambda. \tag{5}$$

Here, $\lambda$ is the incident light wavelength and the extinction coefficient $k$ is extracted from $\varepsilon^{\perp}_{\text{VACNT}}$ [31].

## 3. Results and discussion

### 3.1. Experimental results

Figure 2 shows the cross-sectional scanning electron microscopy (SEM) images of CNT samples synthesized at different

temperatures. At 480 °C, the sample grown for 3 min (4.81 $\mu$m) in figure 2(a) is taller than the sample grown for 5 min (4.46 $\mu$m) in figure 2(b). At 530 °C, the sample grown for 15 min (12.2 $\mu$m) in figure 2(e) is taller than the sample grown for 20 min (7.45 $\mu$m) in figure 2(f). This indicates that excessive growth time may cause VACNTs to be etched in the H$_2$ ambient. By comparing figures 2(b)–(d), it can be found that under the same growth time of 5 min, the higher the temperature, the taller the CNTs.

We further study the CNT samples by Raman spectroscopy, and the results are shown in figure 3. Raman spectroscopy is a non-destructive testing method that can quickly provide structural information of CNT arrays [32]. Figure 3 shows that these samples have two main peaks: D peak near 1350 cm$^{-1}$ and G peak near 1590 cm$^{-1}$ (see table 1 for details). The origin of D is related to disorder-induced features or defective graphitic structure. Because the bending of the CNTs introduces stacking faults and possibly pentagonal and heptagonal defects, it destroys the integrity of the hexagonal carbon rings, resulting in a strong peak near 1350 cm$^{-1}$. The G peak is related to the tangential stretching (E$_{2g}$) mode of highly oriented pyrolytic graphite, indicating the presence of crystalline graphitic structures in the CNTs. The D peak increases with the increased defects in the CNTs. The intensity ratio of D and G, $I_D/I_G$, which is often used to describe the density of point defects in graphite [33], indicates the extent of disorder in CNTs. The sample grown at 530 °C
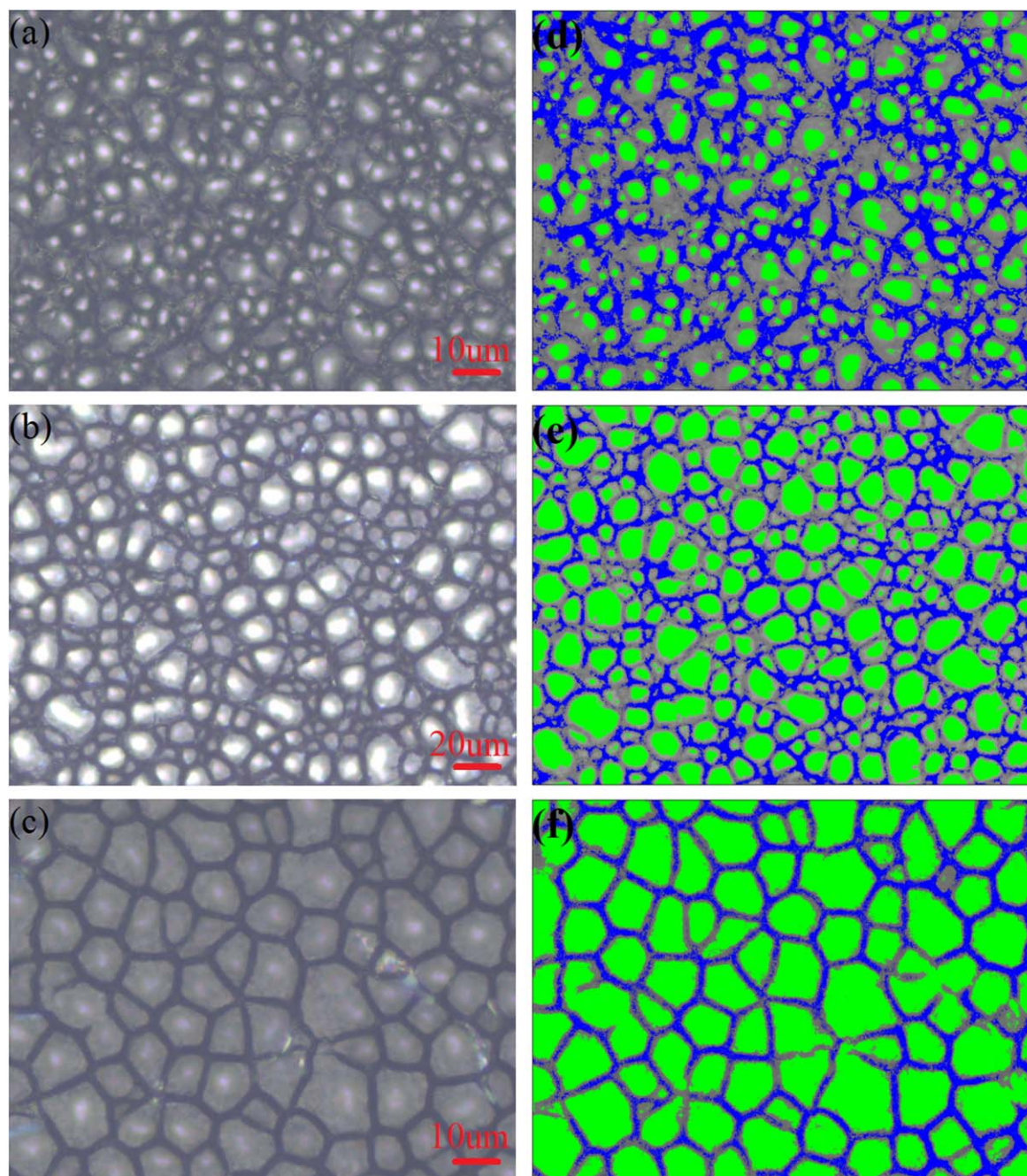
**Figure 4.** (a)–(c) are the top-view images of the CNT samples after liquid-induced compaction. (a) 530 °C for 5 min, (b) 530 °C for 10 min, and (c) 530 °C for 15 min (d)–(f) are the image processing results of (a)–(c), respectively. (d) $f = 0.2725$, (e) $f = 0.1829$, and (f) $f = 0.1357$.

for 10 min has the highest $I_D/I_G$ value of 1.520, indicating that this samples has the lowest degree of graphitization.

We use the LIC method to estimate the fill factor *f* of the CNT samples, which is a destructive technique (figure 4, figure S2-S5). Figures 4(a)–(c) show the optical images of several CNT samples after the LIC process. The CNTs are densified on the surface (the black part in figures 4(a)–(c)). The density of the CNT samples prepared in our study is low, each of which forms a cellular structure that agrees with previous research of low-density CNT forests [34–36]. Further, the fill factor is obtained through image processing. Figures 4(d)–(f) show the image processing results of

figures 4(a)–(c), respectively, in which the green part is the exposed substrate at the bottom, and the blue part is the densified CNT on top. The fill factor is the pixel ratio of the blue part to the total image, and the calculated values are given in the figure caption.

We measure the transmittance *T* of the samples using FTIR (figure S6), and then obtain the absorbance using $A = 1 - T$ (figure S7). In the near-infrared to the mid-infrared region (wavelength from 2.5 to 25 $\mu$m), the sample grown at 580 °C for 5 min has the highest absorbance, reaching 87.8%. This important high-absorption characteristic stems from the unique forest structure of CNT arrays, where CNTs are
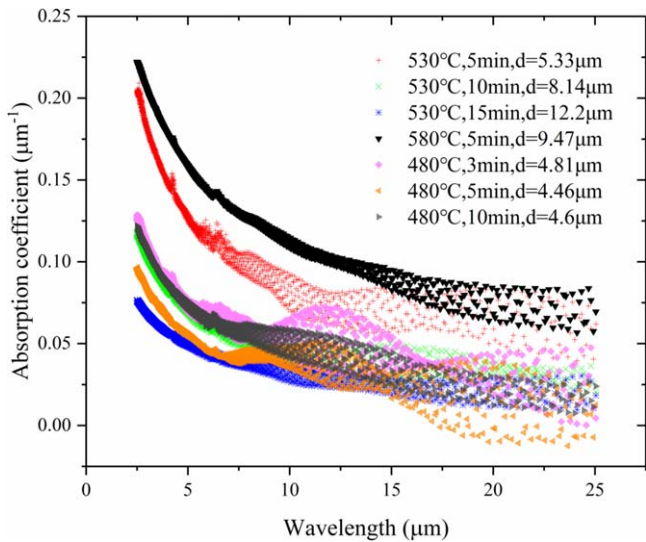
**Figure 5.** Absorption coefficients of CNT samples obtained from measured transmittance.

sparsely distributed across the sample and vertically aligned to various extents [18]. Thus, both the fill factor $f$ and the alignment factor $x$ affect the absorption. At 530 °C, the absorbance of the sample grown for 5 min (66.3%) is higher than that of the sample grown for 15 min (60.6%). At 480 °C, the absorbance of the sample grown for 3 min (46.1%) is higher than that of the sample grown for 5 min (34.9%). This shows that for the same growth temperature, longer growth time results in lower absorption, supporting the probable cause being increased etching due to prolonged growth in the $H_2$ ambient. On the other hand, when the growth time is 10 min, the absorbance of the sample grown at 530 °C (61.7%) is higher than that of the sample grown at 480 °C (42.7%). When the growth time is at 5 min, the absorbance of samples grown at different temperatures follows this pattern: 34.9% (480 °C) < 66.3% (530 °C) < 87.8% (580 °C). Thus, for the same growth time, a higher growth temperature within this range leads to higher absorption. This finding is consistent with the results in figure 2, showing that under the same growth time of 5 min, the higher the temperature, the taller the CNTs, which results in higher absorption.

### 3.2. Analysis of experimental results

The absorption coefficient is a critical parameter for optimizing the film thickness in radiometric and other applications. Considering the low reflectance and high absorbance of the CNT film, we can experimentally determine the absorption coefficient from the CNT transmittance $T_{CNT}$ using [21]

$$\alpha_\lambda = -\frac{1}{d} \ln(T_{CNT}), \qquad (6)$$

where $T_{CNT}$ is obtained using FTIR and $d$ is the film thickness which can be measured from SEM images in figure 2. $T_{CNT}$ depends on several factors including $d$. Results of absorption coefficients for the VACNT array samples obtained using equation (6) are shown in figure 5. We note the peaks at ~4 and 6.5 $\mu$m in figure 5. The transmittance $T_{CNT}$ in equation (6)

is measured with a FTIR spectrometer at room temperature. While the spectrometer was purged with $N_2$ gas, residual absorptions by $CO_2$ (at wavelength ~4 $\mu$m) and by water vapor (6.5 $\mu$m) were probably the cause for those peaks. The two samples grown at 480 °C for 3 and 5 min also show a broad peak around 12 $\mu$m, which may be due to possible phonon-assisted infrared absorption in CNTs, and determination of its exact origin requires further investigation in future studies. We observe that $\alpha_\lambda$ does not always increase with increasing $d$. The results show that VACNT arrays with a 9.47 $\mu$m film thickness has the highest absorption coefficient throughout the entire wavelength range. It appears that the thickness of the film can be optimized to achieve better absorption and a smaller thermal mass, which is critical for its application in bolometers.

Based on the analysis outlined in section 2.2, we calculate the absorption coefficient of the VACNT arrays with different fill factor $f$ and alignment factor $x$. We then examine the dependence of the absorption coefficient $\alpha_\lambda$ on $f$ and $x$. According to the results of the LIC process (see figure 4 and supporting information for details (available online at stacks. iop.org/NANO/32/505719/mmedia)), the measured value of $f$ ranges from 0.1357 to 0.2725. Thus, we select $f = 0.15$, 0.20, and 0.25 for our calculations and comparison with the experiment. Previous studies stated that for typical CVD-grown CNT samples, the best-fitted values of the alignment factor were $x = 0.955$, 0.969, and 0.980 [21], which we use for our calculations. The results are shown in figure 6. It can be seen from figures 6(a)–(c) that when $f$ is fixed, $\alpha_\lambda$ increases as $x$ decreases. This is attributed to the slight reduction in alignment resulting in significant decrease in transmittance due to increased light scattering within the CNT layer, leading to increase in absorption [18]. Figures 6(d)–(f) show that with the same $x$, $\alpha_\lambda$ increases as $f$ increases, consistent with higher CNT array density resulting in enhanced absorption.

Based on our analysis, we fit the experimental absorption data of the CNT samples to our calculated values using $f$ and $x$ as fitting parameters, and the results are shown in figure 7 and figures S8–S10. The solid lines represent the calculation results, with the experimental data are denoted by points. Both sets of results exhibit the same trend. In the EMT simulation (solid lines), there exist sharp CNT phonon features at 6.5 and 11.5 $\mu$m. Previous research pointed out that these modes often exist in single-walled CNTs but can be suppressed in multi-walled CNTs [21]. However, it is unclear whether MWCNTs can completely suppress these peaks. The experimental data shown in figure 7 reveal that these two peaks still exist (albeit with reduced intensities). The peak at 6.5 $\mu$m is likely due largely to water vapor (see figure 5 and its related discussion), with possible contribution from CNT phonon, and the peak at 11.5 $\mu$m probably results from phonon absorption in single-walled CNTs present in the samples. The best-fit values of $f$ and $x$ are shown in the figures, and the measured values of $f$ are given in the figure caption. Figure 7(a) shows the fitted absorption coefficient of the sample grown at 530 °C for 5 min, with the fitting parameters $f = 0.2758$ and $x = 0.9954$. For this sample, we measure $f = 0.2725$ using the LIC method (see figure 4(d)),
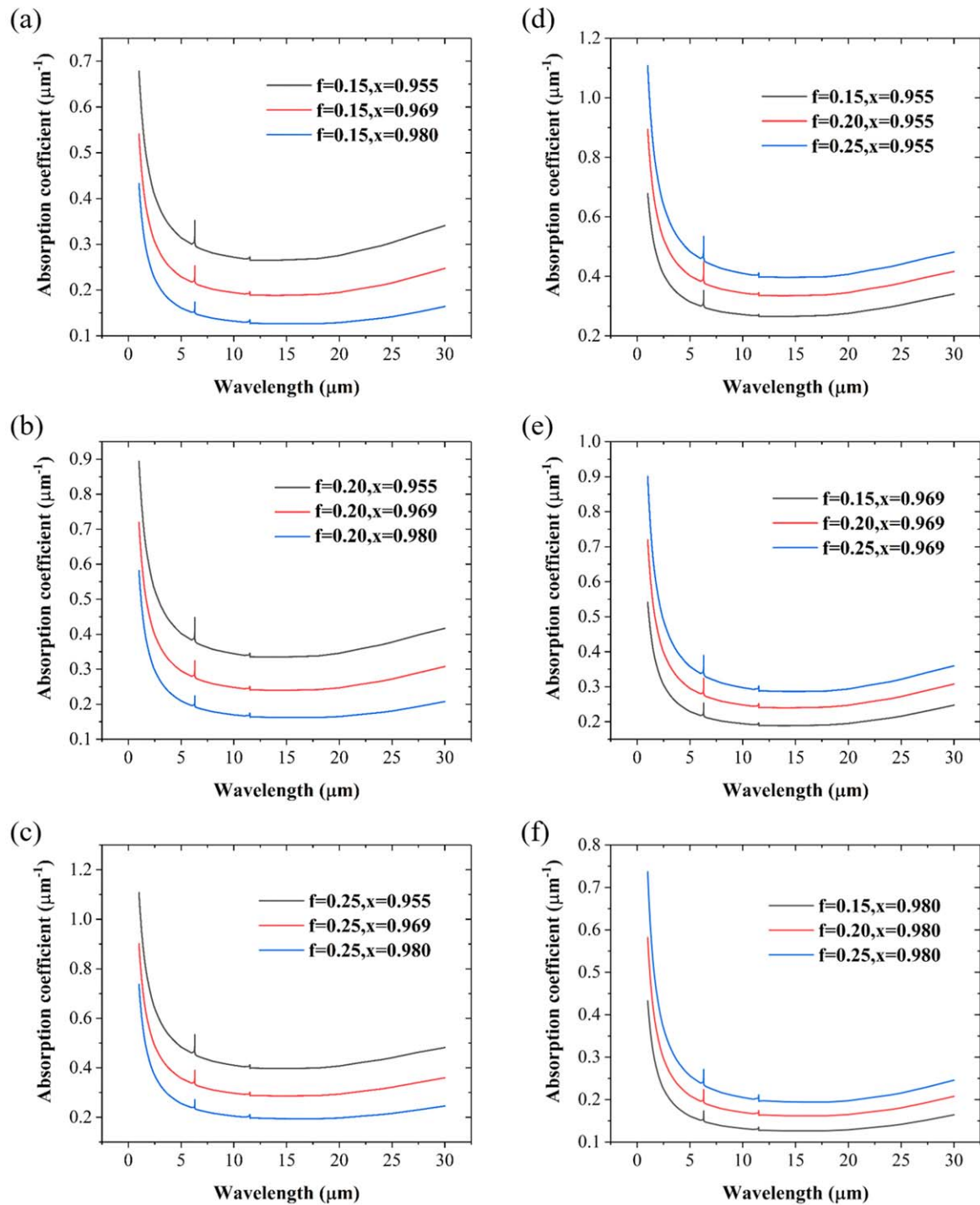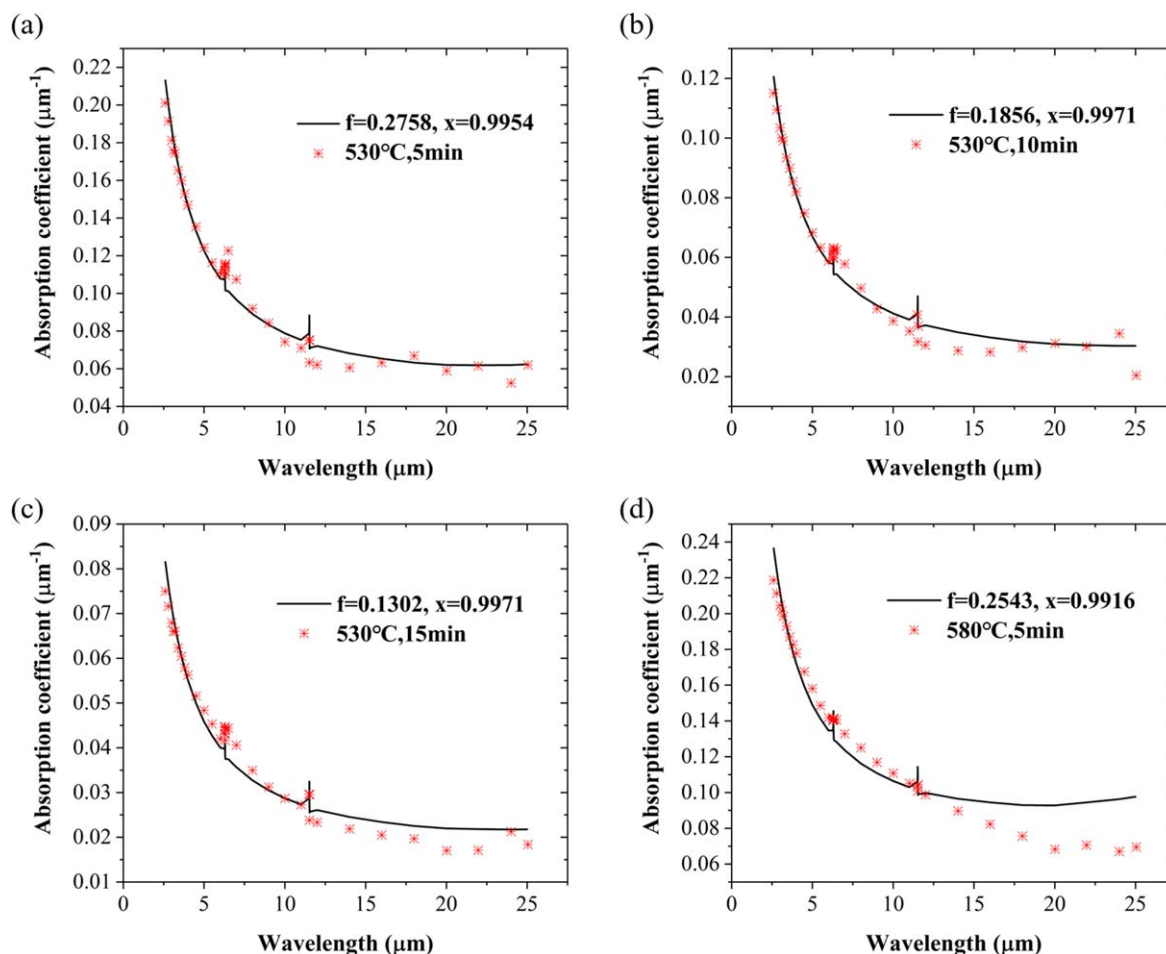
**Figure 6.** Calculated absorption coefficients. (a)–(c) fixed *f* for various *x*, (d)–(f) fixed *x* for various *f*.

indicating a very close match with the fitted *f* value. For a sample grown at 530 °C for 10 min, as shown in figure 7(b), the fitted $f = 0.1856$ also matches very well with the measured $f = 0.1829$ (see figure 4(e)). Figure 7(c) shows the fitting result of the sample at 530 °C for 15 min. The fitted $f = 0.1302$ also matches the measured $f = 0.1357$ (see figure 4(f)). It can be seen from figures 7(a)–(c) that a longer growth time reduces *f*, resulting in a smaller absorption coefficient, as alluded to previously.

Figure 7(d) shows that the absorption coefficient of the sample grown at 580 °C for 5 min is moderately higher than that for a sample grown at 530 °C for 5 min shown in figure 7(a), for the same range of wavelengths. However, the fill factor of the former sample is slightly lower (measured 0.2571 versus 0.2725 and fitted 0.2543 versus 0.2758). Thus, the higher growth temperature yields a slightly less dense CNT array but a larger absorption coefficient. On the other hand, the CNT grown at 580 °C for 5 min is significantly

**Figure 7.** Fitting of calculated results to measured absorption coefficient data. The solid lines represent the calculated results and the points represent the experimental data. (a) 530 °C for 5 min, fitted $f = 0.2758$; measured $f = 0.2725$ (figure 4(d)). (b) 530 °C for 10 min, fitted $f = 0.1856$; measured $f = 0.1829$ (figure 4(e)). (c) 530 °C for 15 min, fitted $f = 0.1302$; measured $f = 0.1357$ (figure 4(f)). (d) 580 °C for 5 min, fitted $f = 0.2543$; measured $f = 0.2571$ (figure S2).

**Table 2.** Process parameters and the absorption performances of the CNT samples.

| Growth temperature (°C) | Growth time (min) | CNT height $d$ ($\mu$m) | Fill factor $f$ (LIC) | Absorbance ($\lambda = 2.5\ \mu$m) | Absorption coefficient $\alpha_\lambda$ ($\mu$m$^{-1}$) ($\lambda = 2.5\ \mu$m) |
|---|---|---|---|---|---|
| 530 | 5 | 5.33 | 0.2725 | 0.663 458 | 0.204 321 |
| 530 | 10 | 8.14 | 0.1829 | 0.616 894 | 0.117 868 |
| 530 | 15 | 12.2 | 0.1357 | 0.605 747 | 0.076 292 |
| 580 | 5 | 9.47 | 0.2571 | 0.877 971 | 0.222 122 |
| 480 | 3 | 4.81 | 0.1812 | 0.461 107 | 0.128 532 |
| 480 | 5 | 4.46 | 0.1599 | 0.348 765 | 0.096 162 |
| 480 | 10 | 4.60 | 0.1799 | 0.427 161 | 0.121 12 |

taller than the CNT grown at 530 °C for 5 min (9.47 $\mu$m versus 5.33 $\mu$m), as shown in figures 2(c) and (d). The higher absorption coefficient of the sample grown at 580 °C is likely a result of the competing effects of the CNT height and its array density. In this case, the significantly taller CNTs seem to be the dominant determining factor for increased absorption.

Currently, there is no effective measurement technique for the alignment factor *x*. The results show that for long wavelengths, experimental data agree less well with

calculated values of absorption coefficient, probably due to the presence of significant noise in FTIR measurements at lower frequencies. Nevertheless, the comparisons between theory and experiment in much of the infrared spectrum are encouraging and lay the groundwork for further assessing the utility of CNT as an effective infrared absorption material.

Table 2 summarizes the physical parameters and the absorption performances of the CNT array samples. The dependence of absorption coefficient on the fill factor and CNT height is shown in figure S11. The samples grown at

530 °C and 580 °C for 5 min exhibit a relatively large absorption coefficient ($>0.20\ \mu m^{-1}$), while the CNT array height of the latter sample is almost twice that of the former. This result suggests that the lower temperature process does not diminish the absorption performance.

## 4. Conclusions

Prior research has shown that VACNT can absorb incident light almost perfectly in a very wide spectral range ($0.2–200\ \mu m$) [18]. This high absorption characteristic similar to black body is due to the VACNT's unique forest structure, in which the vertically aligned CNTs are distributed evenly and sparsely. Such studies showed that in order to obtain an almost constant absorbance close to 1 in the infrared range, the thickness of the CNT film needed to be greater than 50 $\mu$m. This resulted in a large thermal mass, and bolometers with such thick CNT film as its absorption layer would have a slow response rate.

In this study, relatively thin CNT films ($\sim10\ \mu m$ or less) are prepared using PECVD with a low growth temperature ($\sim500\ °C$) and a short growth time (5–15 min). The transmittances of various samples are measured using FTIR, and the absorption characteristics are obtained. We also use EMT and MGA methods to model the absorption behavior of CNT films in the infrared region using the anisotropic optical constants of graphite. The absorption coefficients $\alpha_\lambda$ of the CNT film for different filling factor $f$ and alignment factor $x$ are calculated. Our measured and calculated absorption coefficients agree well, and both show consistently that the larger the fill factor $f$, the better the absorption. The calculations also reveal that within the range of $f$ between 0.15 and 0.25, a smaller degree of misalignment with $x$ slightly below 1 is actually more conducive to increasing the CNT absorption, probably due to increased light refraction inside the CNT film.

Measurement with FTIR identifies the CNT array grown at 580 °C for 5 min as having the highest absorbance of 87.8%. This 9.47 $\mu$m thick sample with a fill factor of 0.2571 is not the thickest or the densest of all samples, but it has the highest absorption coefficient $\alpha_\lambda$ in the entire range of wavelengths. Our results show that a slightly elevated temperature combined with moderate growth time can yield a CNT array with sufficient height and array density to achieve a high absorbance among all the samples with various array densities. In fabricating vertical CNT arrays for a given growth time, increasing the growth temperature can increase the CNT height, leading to higher absorption. On the other hand, too long a growth time can cause the nanotubes to collapse and entangle, failing to form the structure necessary to absorb light effectively. Therefore, an optimal combination of growth time and temperature appears to exist, and needs to be explored further. We plan to expand the current investigation to study the integration of a CNT infrared absorption layer with a two-dimensional array of photothermal infrared detectors. Toward that end, we have identified in this study PECVD CNT films that demonstrate reasonable infrared absorption with relatively low thermal mass, which can potentially be integrated with resonators or other optoelectronic device structures.

## Data availability statement

The data that support the findings of this study are available upon reasonable request from the authors.

## ORCID iDs

Changjian Zhou ⓘ https://orcid.org/0000-0002-7156-348X

## References

[1] Kimata M 2018 Uncooled infrared focal plane arrays *IEEJ Trans. Electr. Electron. Eng.* **13** 4–12
[2] Rogalski A 2011 Recent progress in infrared detector technologies *Infrared Phys. Technol.* **54** 136–54
[3] Lang W, Kühl K and Sandmaier H 1992 Absorbing layers for thermal infrared detectors *Sensors Actuators* A **34** 243–8
[4] Muralt P 2001 Micromachined infrared detectors based on pyroelectric thin films *Rep. Prog. Phys.* **64** 1339
[5] Murphy D *et al* 2007 640 × 512 17 $\mu$m microbolometer FPA and sensor development *Infrared Technology and Applications XXXIII Proc. SPIE* vol 6542, 65421Z
[6] Niklaus F, Vieider C and Jakobsen H 2008 MEMS-based uncooled infrared bolometer arrays: a review *MEMS/ MOEMS Technologies and Applications III Proc. SPIE* vol 6836, p 68360D
[7] Chirila C, Botea M, Iuga A, Tomulescu A, Balescu L, Galca A, Boni A, Leonat L, Pintilie I and Pintilie L 2019 Carbon-based sprayed electrodes for pyroelectric applications *PLoS One* **14** e0221108
[8] Lehman J, Theocharous E, Eppeldauer G and Pannell C 2003 Gold-black coatings for freestanding pyroelectric detectors *Meas. Sci. Technol.* **14** 916
[9] Steglich M, Lehr D, Ratzsch S, Käsebier T, Schrempel F, Kley E B and Tünnermann A 2014 An ultra-black silicon absorber *Laser Photon. Rev.* **8** L13–7
[10] Smith E M, Panjwani D, Ginn J, Warren A P, Long C, Figuieredo P, Smith C, Nath J, Perlstein J and Walter N 2016 Dual band sensitivity enhancements of a VOx microbolometer array using a patterned gold black absorber *Appl. Opt.* **55** 2071–8
[11] Suen J Y, Fan K, Montoya J, Bingham C, Stenger V, Sriram S and Padilla W J 2017 Multifunctional metamaterial pyroelectric infrared detectors *Optica* **4** 276–9
[12] Wang J, Li Y, Deng L, Wei N, Weng Y, Dong S, Qi D, Qiu J, Chen X and Wu T 2017 High-performance photothermal conversion of narrow-bandgap $Ti_2O_3$ nanoparticles *Adv. Mater.* **29** 1603730

[13] Stephens M *et al* 2021 Room temperature laser power standard using a microfabricated, electrical substitution bolometer *Rev. Sci. Instrum.* **92** 025107

[14] Lehman J, Yung C, Tomlin N, Conklin D and Stephens M 2018 Carbon nanotube-based black coatings *Appl. Phys. Rev.* **5** 011103

[15] Nandi S and Misra A 2020 Spray coating of two-dimensional suspended film of vanadium oxide-coated carbon nanotubes for fabrication of a large volume infrared bolometer *ACS Appl. Mater. Interfaces* **12** 1315–21

[16] Jönsson M, Nerushev O A and Campbell E E B 2007 *In situ* growth rate measurements during plasma-enhanced chemical vapour deposition of vertically aligned multiwall carbon nanotube films *Nanotechnology* **18** 305702

[17] Theocharous E, Theocharous S and Lehman J 2013 Assembly and evaluation of a pyroelectric detector bonded to vertically aligned multiwalled carbon nanotubes over thin silicon *Appl. Opt.* **52** 8054–9

[18] Mizuno K, Ishii J, Kishida H, Hayamizu Y, Yasuda S, Futaba D N, Yumura M and Hata K 2009 A black body absorber from vertically aligned single-walled carbon nanotubes *Proc. Natl Acad. Sci.* **106** 6044–7

[19] Theocharous S, Theocharous E and Lehman J 2012 The evaluation of the performance of two pyroelectric detectors with vertically aligned multi-walled carbon nanotube coatings *Infrared Phys. Technol.* **55** 299–305

[20] De Nicola F, Hines P, De Crescenzi M and Motta N 2017 Thin randomly aligned hierarchical carbon nanotube arrays as ultrablack metamaterials *Phys. Rev.* B **96** 045409

[21] Ye H, Wang X, Lin W, Wong C and Zhang Z 2012 Infrared absorption coefficients of vertically aligned carbon nanotube films *Appl. Phys. Lett.* **101** 141909

[22] Zhang R Z, Liu X and Zhang Z M 2015 Modeling the optical and radiative properties of vertically aligned carbon nanotubes in the infrared region *J. Heat Transfer* **137** 9

[23] Maschmann M R, Amama P B, Goyal A, Iqbal Z, Gat R and Fisher T S 2006 Parametric study of synthesis conditions in plasma-enhanced CVD of high-quality single-walled carbon nanotubes *Carbon* **44** 10–8

[24] Zhong G, Xie R, Yang J and Robertson J 2014 Single-step CVD growth of high-density carbon nanotube forests on metallic Ti coatings through catalyst engineering *Carbon* **67** 680–7

[25] Garcia-Vidal F, Pitarke J and Pendry J 1997 Effective medium theory of the optical properties of aligned carbon nanotubes *Phys. Rev. Lett.* **78** 4289

[26] Lü W, Dong J and Li Z-Y 2000 Optical properties of aligned carbon nanotube systems studied by the effective-medium approximation method *Phys. Rev.* B **63** 033401

[27] Maxwell-Garnett J C 1904 Colours in metal glasses and in metallic films *Phil. Trans. R. Soc.* A **203** 385–420

[28] Draine B 1985 Tabulated optical properties of graphite and silicate grains *Astrophys. J. Suppl. Ser.* **57** 587–94

[29] Wang X, Flicker J, Lee B J, Ready W and Zhang Z 2009 Visible and near-infrared radiative properties of vertically aligned multi-walled carbon nanotubes *Nanotechnology* **20** 215704

[30] Bao H, Ruan X and Fisher T S 2010 Optical properties of ordered vertical arrays of multi-walled carbon nanotubes from FDTD simulations *Opt. Express* **18** 6347–59

[31] Zhang Z M 2020 *Nano/Microscale Heat Transfer* (Berlin: Springer)

[32] Dresselhaus M S, Dresselhaus G, Saito R and Jorio A 2005 Raman spectroscopy of carbon nanotubes *Phys. Rep.* **409** 47–99

[33] Tuinstra F and Koenig J L 1970 Raman spectrum of graphite *J. Chem. Phys.* **53** 1126–30

[34] Chakrapani N, Wei B, Carrillo A, Ajayan P M and Kane R S 2004 Capillarity-driven assembly of two-dimensional cellular carbon nanotube foams *Proc. Natl Acad. Sci.* **101** 4009–12

[35] Correa-Duarte M A, Wagner N, Rojas-Chapana J, Morsczeck C, Thie M and Giersig M 2004 Fabrication and biocompatibility of carbon nanotube-based 3D networks as scaffolds for cell seeding and growth *Nano Lett.* **4** 2233–6

[36] Liu H, Li S, Zhai J, Li H, Zheng Q, Jiang L and Zhu D 2004 Self-assembly of large-scale micropatterns on aligned carbon nanotube films *Angew. Chem., Int. Ed.* **43** 1146–9